Biochimica et Biophysica Acta 1794 (2009) 642–654

Contents lists available at ScienceDirect

Biochimica et Biophysica Acta

journal homepage: www.elsevier.com/locate/bbapap

Elucidation of the substrate specificity, kinetic and catalytic mechanism of adenylosuccinate lyase from *Plasmodium falciparum*

Vinay Bulusu, Bharath Srinivasan, Monnanda Ponnappa Bopanna, Hemalatha Balaram *

Molecular Biology and Genetics Unit, Jawaharlal Nehru Centre for Advanced Scientific Research, Jakkur, Bangalore, 560 064, India

ARTICLE INFO

Article history:
Received 20 September 2008
Received in revised form 21 November 2008
Accepted 24 November 2008
Available online 7 December 2008

Keywords:
Plasmodium falciparum
Adenylosuccinate lyase
Catalysis
Rapid equilibrium
AICAR

ABSTRACT

Adenylosuccinate lyase (ASL) catalyzes two distinct but chemically similar reactions in purine biosynthesis. The first, exclusive to the de novo pathway involves the cleavage of 5-aminoimidazole-4-(N-succinylcarboxamide) ribonucleotide (SAICAR) to 5-aminoimidazole-4-carboxamide ribonucleotide (AICAR) and fumarate and the second common to both de novo and the salvage pathways involves the cleavage of succinyl-adenosine monophosphate (SAMP) to AMP and fumarate. A detailed kinetic and catalytic mechanism of the recombinant His-tagged ASL from *Plasmodium falciparum* (PfASL) is presented here. Initial velocity kinetics, product inhibition studies and transient kinetics indicate a Uni-Bi rapid equilibrium ordered mechanism. Substrate and solvent isotope effect studies implicate the process of C(γ)–N bond cleavage to be rate limiting. Interestingly, the effect of pH on k_{cat} and k_{cat}/K_m highlight ionization of the base only in the enzyme substrate complex and not in the enzyme alone, thereby implicating the pivotal role of the substrate in the activation of the catalytic base. Site-directed mutagenesis implicates a key role for the conserved serine (S298) in catalysis. Despite the absence of a de novo pathway for purine synthesis and most importantly, the absence of other enzymes that can metabolise AICAR in *P. falciparum*, PfASL catalyzes the SAICAR cleavage reaction with kinetic parameters similar to those of SAMP reaction and binds AICAR with affinity similar to that of AMP. The presence of this catalytic feature allows the use of AICAR or its analogues as inhibitors of PfASL and hence, as novel putative anti-parasitic agents. In support of this, we do see a dose dependent inhibition of parasite growth in the presence of 5-aminoimidazole-4-carboxamide ribonucleoside (AICAriboside) with half-maximal inhibition at 167±5 μM.

1. Introduction

Adenylosuccinate lyase (ASL)[2] (E.C. 4.3.2.2) is the only enzyme in the purine biosynthetic pathway that catalyzes two distinct, but chemically similar reactions. The first is the cleavage of 5-aminoimidazole-4(N-succinylcarboxamide) ribonucleotide (SAICAR) to 5-aminoimidazole-4-carboxamide ribonucleotide (AICAR) and fumarate that forms the eighth step of the *de novo* purine biosynthetic pathway and the second being the cleavage of succinyl-adenosine monophosphate (SAMP) to adenosine monophosphate (AMP) and fumarate, the final step in AMP synthesis [1] (Fig. 1). Previous studies have indicated that ASLs from *Bacillus subtilis* [2], *Neurospora crassa* [3] and *Homo sapiens* [4] are able to act upon both the substrates with equal efficiency.

ASL is a member of a superfamily of enzymes that includes class II fumarase, aspartase, arginosuccinate lyase, etc. Members of this family have high structural similarity [5–9] despite their low amino acid sequence identity, catalyze β elimination reactions and possess the signature sequence "SSxxPxKxNxxxxE", where 'X' represents any amino acid. Each member of this family is a homotetramer with a molecular mass of approximately 200 kDa. Earlier, the cleavage of SAMP to AMP and fumarate by ASL has been shown to follow an ordered Uni-Bi mechanism in which fumarate leaves the enzyme first followed by AMP. It has been proposed that the overall rate is determined by a step that follows catalysis [10]. ASL catalysis involves the attack by a general base on the methylene proton at the β position of succinyl group (C(β)–H) of SAMP followed by the protonation of the imino nitrogen by a general acid leading to the formation of AMP and fumarate. In *B. subtilis* ASL, a conserved histidine (H141) has been shown to play the role of the catalytic base [11] while another conserved histidine (H68) has been implicated as the catalytic acid [12]. However, this earlier accepted role of histidines in catalysis has been altered subsequent to the solving of the liganded and unliganded crystal structures of *E. coli* ASL [13]. The conserved histidine (H171) that was originally thought to be the base seems to be acting as an acid due to its proximity to the imino group of SAMP while a conserved

Abbreviations: ASL, adenylosuccinate lyase; PfASL, *Plasmodium falciparum* ASL; DTT, dithiothreitol; IC_{50}, 50% inhibitory concentration; SAICAR, 5-aminoimidazole-4-(N-succinylcarboxamide) ribonucleotide; AICAR, 5-aminoimidazole-4-carboxamide ribonucleotide; AICAriboside, 5-aminoimidazole-4-carboxamide ribonucleoside; SAMP, succinyl-adenosine monophosphate; KIE, kinetic isotope effect; ITC, isothermal titration calorimetry

* Corresponding author. Tel.: +91 80 22082812; fax: +91 80 22082766.
E-mail address: hb@jncasr.ac.in (H. Balaram).

1570-9639/$ – see front matter © 2008 Elsevier B.V. All rights reserved.
doi:10.1016/j.bbapap.2008.11.021

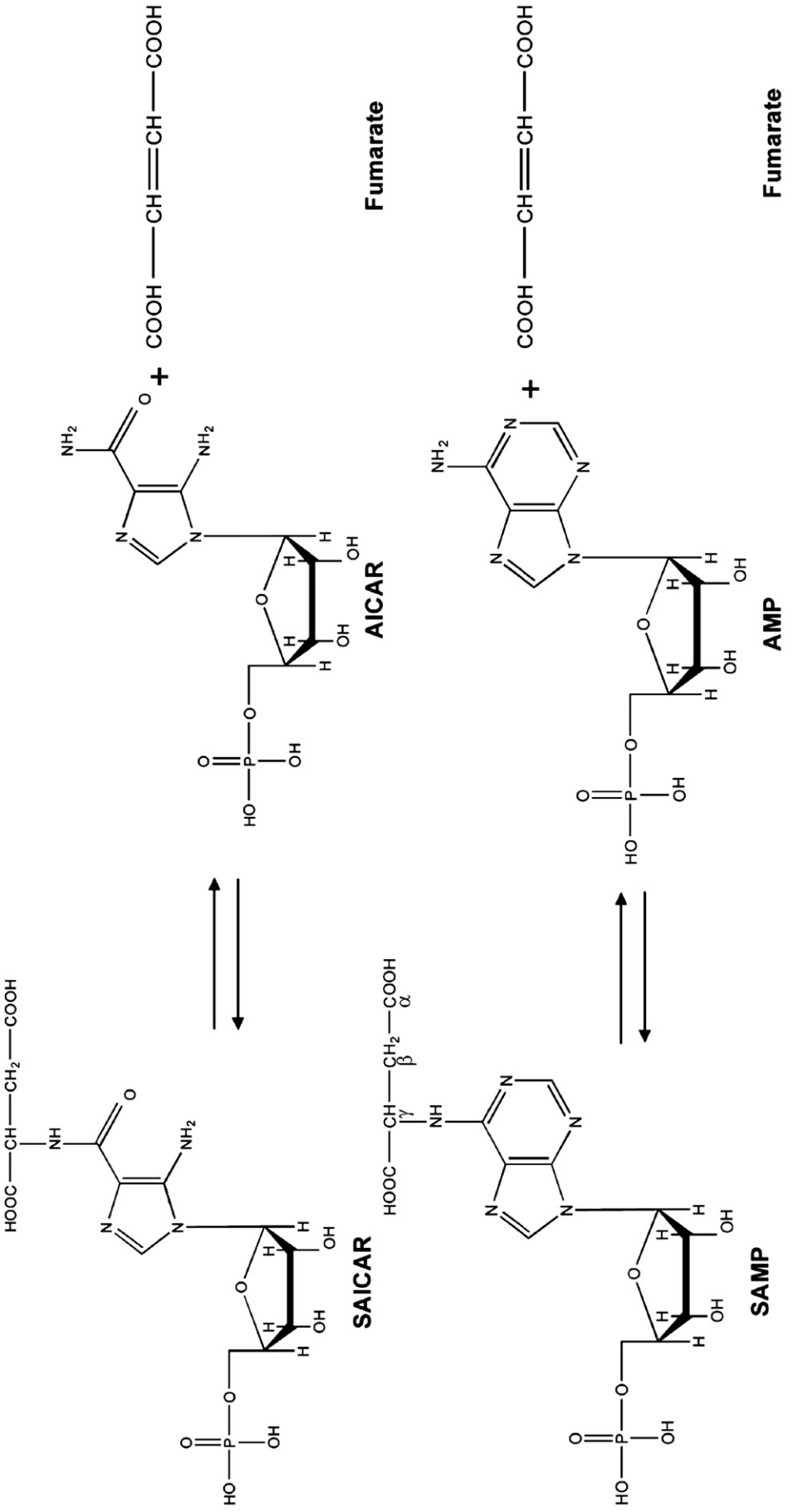

Fig. 1. Reactions catalysed by adenylosuccinate lyase.

serine (S295) has been proposed to be the catalytic base owing to its proximity to the C(β)–H of SAMP.

Plasmodium falciparum and most other parasitic protozoa lack the *de novo* purine biosynthetic pathway and depend solely on the salvage pathway for their purine requirements [14]. In view of this, it is not known if PfASL has retained SAICAR activity. The pathway operates through the salvage of hypoxanthine from the host that is phosphoribosylated to IMP by hypoxanthine guanine phosphoribosyltransferase. IMP is converted to GMP by the action of IMP dehydrogenase and GMP synthetase and, to AMP by adenylosuccinate synthetase and ASL. In *P. falciparum*, AMP synthesis seems to depend solely on the concerted action of adenylosuccinate synthetase and adenylosuccinate lyase as no other alternate routes for its synthesis have been found [15]. This is supported by the finding that hadacidin, a highly specific and potent inhibitor of adenylosuccinate synthetase [16] inhibits parasite growth under in vitro conditions [17]. An earlier report by Marshall *et al.* [18] shows significant sequence divergence of *P. falciparum* ASL (PfASL) from the human homolog. Hence, PfASL has been proposed to be a putative target for anti-malarial drug development and this necessitates its detailed kinetic and biochemical characterization.

We report here the detailed biochemical and kinetic characterization of recombinant PfASL. Our results from initial velocity kinetics, product inhibition, equilibrium ligand binding and transient kinetics show that PfASL catalysis involves an ordered release of products, but under rapid equilibrium and not the proposed steady state conditions. The overall rate of the reaction is dictated by the catalytic step and more specifically, the C–N bond cleavage in the substrate. Interestingly, for the first time in any of the ASLs reported, PfASL shows a dramatic decrease in the pK_a value of its catalytic base upon SAMP binding. Finally, we show that PfASL acts on both SAICAR and SAMP with similar thermodynamic and kinetic constants. In view of the absence of a de novo biosynthetic pathway for purine synthesis, the extended substrate specificity of PfASL could be used in the development of AICAR or its analogues as novel anti-malarial drugs. In support of this, our studies also show that the cell permeable AICAriboside inhibits the parasite growth in culture.

2. Materials and methods

2.1. Materials

All chemical reagents used were of high quality and obtained from Sigma Chemicals Co., USA. Restriction enzymes, *Pfx* DNA polymerase and T4 DNA ligase were from Invitrogen, USA and Bangalore Genei Pvt. Ltd., India and were used according to the manufacturers' instructions. Gel filtration matrices were from Amersham Biosciences, UK. Primers were custom synthesized at Microsynth, Switzerland. Media components were from Himedia, Mumbai, India.

2.2. Cloning, expression and purification of PfASL

PfASL gene was amplified using parasite genomic DNA as template and with a forward primer (5′GCTCCATGGATCCACATGTGAACCAACTGAAAAAC3′) with *Nco*I and *Bam*HI and a reverse primer (5′ACTCGAGTATATTCCTGTGAGAAGTGCTC3′) with *Hin*dIII and *Xho*I restriction sites. A nonconserved valine was substituted with proline (V3P) to facilitate the introduction of *BamH* I site. Amplification yielded a single DNA fragment corresponding to 1.4 kb that was digested with *Nco*I and *Xho*I and cloned in pET28b expression vector. The identity of the clone was confirmed by sequencing. The protein was expressed with a hexahistidine tag at the C-terminus in *E. coli* BL21-CodonPlus™ (DE3)-RIL cells (Stratagene, USA). Transformed cultures were grown in terrific broth containing kanamycin (50 μg ml^{-1}) and chloramphenicol (40 μg ml^{-1}) and induced with IPTG at a final concentration of 0.75 mM. Induction was carried out at 16 °C for 12 h. For protein purification, the cell pellets were resuspended in lysis buffer containing 50 mM potassium phosphate, pH 7.4, 100 mM NaCl, 2 mM dithiothreitol (DTT) and 10% glycerol, lysed using French press and centrifuged. The supernatant was incubated with nickel nitrilotriacetic acid agarose beads after which the beads were washed extensively with wash buffer (50 mM potassium phosphate, pH 7.4, 100 mM NaCl, 30 mM imidazole, 2 mM DTT, 10% glycerol). Bound PfASL was eluted with elution buffer, pH 7.4 (wash buffer containing 200 mM imidazole). The eluted protein was concentrated and further purified on Sephacryl 200 gel filtration column pre-equilibrated with 50 mM potassium phosphate, pH 7.4, 100 mM NaCl, 2 mM DTT, 1 mM EDTA and 10% glycerol. The eluted protein was again concentrated and used for further experiments. Protein concentrations were determined by the method of Bradford [19] with bovine serum albumin as a protein standard. Oligomeric status of PfASL was determined at 25 °C using a pre-calibrated Sephacryl S-300 gel filtration column in buffer containing 50 mM sodium phosphate, pH 7.0, and 150 mM NaCl.

2.3. Construction of S298A and S298C PfASL mutants

Site directed mutants of the wild type PfASL were generated by the quick change PCR method using the single mutagenic oligonucleotide method [20]. Primers 5′AAAGAAATTGGCGCGAGTACCATGCCACCATAAAG3′ and 5′AAAGAAATTGGCTGCAGTACCATGCCACCATAAAG 3′ were used for the generation of S298A and S298C mutants, respectively, using wild type gene as template. PCR product was digested with *Dpn*I and transformed into DH5α strain of *E. coli*. The site of mutation was confirmed by DNA sequencing. Conditions for the expression and purification of the mutant proteins were kept same as that for the wild type enzyme.

2.4. Activity measurements

All assays were done in 50 mM potassium phosphate, pH 7.4, in a final reaction volume of 250 μl using a double beam Hitachi UV 2010 spectrophotometer (Hitachi High Technologies America, Inc., San Jose, CA, USA). Enzyme activities were determined using a saturating SAMP concentration of 200 μM in 50 mM potassium phosphate, pH 7.4 at 25 °C. 1 μg of wild type enzyme and 100 μg of the mutant enzymes were used in a final assay volume of 250 μl. Assays were initiated with the addition of substrate to the sample cuvette after zeroing the absorbance reading with respect to the reference cuvette. PfASL activity for SAMP cleavage to AMP and fumarate was monitored as a continuous time dependent decrease in absorbance at 290 nm. Amount of substrate consumed was estimated using the difference extinction coefficient of 4.05 $mM^{-1}cm^{-1}$ [21]. Specific activity was defined as μmoles of substrate converted to product in 1 min by a milligram of enzyme. PfASL activity for SAICAR cleavage to AICAR and fumarate was monitored as a time dependent decrease in absorbance at 267 nm and difference extinction coefficient of 0.7 $mM^{-1}cm^{-1}$ was used to quantitate the amount of substrate consumed [22]. To estimate the kinetic parameters, data was fitted to the Michaelis–Menten equation

$$v = V_{max}[S]/\{K_m + [S]\} \quad (1)$$

Unless mentioned otherwise, all the data were fitted using GraphPad Prism, version 4.0 (GraphPad Software, Inc., San Diego, CA). Assays were done with three different batches of PfASL with each data point being measured in duplicate.

2.5. Order of reaction

2.5.1. Product inhibition

Product inhibition plots were generated by varying SAMP concentrations at fixed concentrations of either AMP or fumarate. K_i values were obtained by non-linear fits to appropriate inhibition

models described below. Standard error and 95% confidence intervals were used as criteria for selecting best fits. The equations for the different inhibitions used were.

Competitive.

$$v = V_{max}[S]/\{K_m(1 + [I]/K_i) + [S]\} \quad (2)$$

Noncompetitive.

$$v = V_{max}[S]/\{K_m(1 + [I]/K_i) + [S](1 + [I]/K_i)\} \quad (3)$$

Uncompetitive.

$$v = V_{max}[S]/\{K_m + [S](1 + [I]/K_i)\} \quad (4)$$

where v is the velocity of the reaction, V_{max} is the maximum velocity, [S] is the substrate concentration, [I] is the inhibitor concentration. K_m is the Michaelis–Menten constant and K_i is the inhibition constant. From the primary linear plot of 1/v versus 1/[SAMP] at different fumarate concentrations, the values for the slopes and the y-intercept were obtained. Secondary plots of slopes versus fumarate concentrations and y-intercept values versus fumarate concentrations were plotted to obtain the inhibition constants K_{is} and K_{ii} respectively.

2.5.2. Initial velocity

Initial velocity plots were generated by varying AMP at different fixed concentrations of fumarate and by varying fumarate at different fixed concentrations of AMP. The maximum concentration of AMP and fumarate was kept at five times the K_m to maintain sub-saturating conditions. The specific activity values obtained at substrate concentrations near the K_m values were approximate values as the measurements were obscured by the approach of equilibrium. However, initial slopes representing less than 10% product formation were taken for the specific activity calculations. A global fit of the data by non-linear regression analysis to the rapid equilibrium ordered bireactant kinetic model was done. The equations used were [23]

$$v = V_{max}[A]/\{K_a(K_b/[B]) + [A](1 + K_b/[B])\} \quad (5)$$

$$v = V_{max}[B]/\{K_b(1 + K_a[A]) + [B]\} \quad (6)$$

where A is the first and B is the second substrate to bind the enzyme E, K_a is the dissociation constant of A from E.A, and K_b is the dissociation constant of B from E.A.B.

2.6. Transient kinetics

Fast reaction kinetics of PfASL in the direction of SAMP cleavage was monitored in a quartz cuvette of pathlength 0.2 cm using a BioLogic SFM 4 stopped flow device (dead time, 10 ms and flow rate, 5 ml s^{-1}) attached to a spectrophotometer (Bio-Logic SAS, France). In order to monitor multiple turnovers, SAMP was maintained at a concentration 20 times greater than the enzyme. Three separate syringes connected to the mixer and the flow cell were filled individually with enzyme, substrate or buffer and incubated at 25 °C for 30 min. The contents of the syringes were mixed in the required amounts to obtain the final concentrations (50 mM potassium phosphate, pH 7.4, 100 μM SAMP and 5 μM PfASL) in the flow cell. Progress of the reaction was monitored as decrease in absorbance at 280 nm with a difference extinction coefficient of 10 $mM^{-1}cm^{-1}$. Each data point was acquired at an interval of 10 ms with the total data acquisition time being 20 s. The plot of turnovers versus time was analyzed by linear regression analysis. Curve fitting was done using GraphPad Prism software, version 4.0.

2.7. SAICAR synthesis

SAICAR was synthesized from AICAR and fumarate as described previously [2], with minor modifications, using PfASL. The reaction was carried out in 50 mM potassium phosphate, pH 7.4, containing 10 mM AICAR, 75 mM fumarate and 0.04 mg of PfASL in a final reaction volume of 1 ml. The reaction mixture was incubated for 4 h at 37 °C. Progress of the reaction was monitored by thin layer chromatography on PEI cellulose with 0.5 M LiCl as the mobile phase [24]. For purification of SAICAR, the reaction mixture was passed through a Microsep® centrifugal device, 10 K cutoff (Pall Life Sciences, USA) to remove the enzyme. The flow-through was loaded on a DEAE anion exchange column and products were eluted with a linear gradient (10–500 mM) of ammonium bicarbonate, pH 8. Under these conditions, SAICAR eluted after AICAR and fumarate. The fraction corresponding to SAICAR was lyophilized, resuspended in water and desalted by passing through Dowex-50W (HCR-W2) cation exchange resin (Sigma Co., USA). The product was confirmed to be SAICAR by mass spectrometry (MALDI-TOF MS, Ultraflex II, Bruker Daltonics, Bremen, Germany) in the positive ion mode.

2.8. Preparation of [^{2}H]-SAMP

[^{2}H] SAMP was synthesized by allowing AMP to react with fumarate in D_2O in the presence of PfASL. Stock solutions of AMP (50 mM) and fumarate (100 mM) were prepared in H_2O. After adjusting the pH of these stock solutions to 7.0, the solutions were lyophilized and redissolved in D_2O. 4 mg of purified PfASL was dialyzed extensively against buffer containing 10 mM Tris, pH 7.4, 10 mM NaCl, and 0.5 mM DTT and lyophilized. The residue was dissolved in D_2O and was again lyophilized. This lyophilized residue, (which retained 90% of the original activity) was added to the reaction mixture in D_2O containing AMP and fumarate at final concentrations of 20 mM and 75 mM, respectively in a total volume of 1 ml. Reaction was allowed to progress for 4 hrs at 37 °C. [^{2}H]SAMP was purified by DEAE-ion exchange chromatography in a similar manner as that for SAICAR. The purified product was analyzed on a Bruker DRX 500 NMR instrument. The spectra indicated >99% deuterium incorporation at the C(β) position of SAMP.

2.9. Solvent isotope effect and proton inventory

PfASL activity was monitored in 50 mM potassium phosphate buffer, pH 7.4 (prepared either in H_2O or D_2O), with varying SAMP concentrations to obtain the kinetic parameters, k_{cat} and K_m. The solvent isotope effect values were calculated as

$$^{D}k_{cat} = k_{cat} \text{ in } H_2O/k_{cat} \text{ in } D_2O$$

$$^{D}k_{cat}/K_m = (k_{cat}/K_m) \text{ in } H_2O/(k_{cat}/K_m) \text{ in } D_2O$$

The lyophilized enzyme was incubated in D_2O for 60 min on ice prior to the assay to allow complete exchange of protons with deuterons. For proton inventory studies, PfASL activity measurements were carried out at different mole fractions of D_2O in H_2O. Data were fitted to the Gross–Butler equation [25] describing a linear proton inventory:

$$^{n}k = {}^{D}k\left(1 - n + n\Phi^{T}\right) \quad (7)$$

where ^nk is the ratio of the rate constants (k_{cat} or k_{cat}/K_m) measured in different fractional concentrations of D_2O compared with 100% D_2O, ^Dk is the solvent deuterium isotope effect (the ratio of the rate constants (k_{cat} or k_{cat}/K_m) in H_2O and D_2O), n is the fractional concentration of D_2O, ϕ^T is the corresponding deuterium fractionation factor for the exchangeable protonic sites relative to bulk water.

2.10. Isothermal titration calorimetry

Binding constants and the associated thermodynamic parameters were determined using a VP-isothermal titration calorimeter (ITC) (Microcal, Inc., Northampton, MA, USA). PfASL was extensively dialyzed against 50 mM potassium phosphate (pH 7.4) containing 100 mM NaCl, 10% glycerol and 1 mM EDTA prior to use. Stock solutions of ligands were made in the same buffer. Titrations were done at 25 °C by stepwise addition of small volumes (5 μl) of ligand stock (AMP or AICAR, at a concentration of 5 mM) to PfASL (160 μM) in the sample cell. A control experiment was performed in which the ligands at the same concentration were titrated against buffer alone in the sample cell in order to obtain the heat of dilution. The raw calorimetric signals were integrated and corrected for the heat of dilution of AMP and AICAR. The resulting corrected binding isotherms were subjected to nonlinear least squares analysis using ORIGIN software and fit to a single-site model to obtain the association constant, $K_{assoc.}$, the binding enthalpy, ΔH^o, and the stoichiometry of the interaction, n. The Gibbs free energy, ΔG^o and the dissociation constant $K_{dissoc.}$ were calculated using the following equations:

$$\Delta G^o = \Delta H^o - T\Delta S \tag{8}$$

$$K_{dissoc} = 1/K_{assoc}. \tag{9}$$

2.11. pH kinetics

pH dependence of PfASL specific activity was monitored over the pH range 6.0–9.0 with varying SAMP concentrations. The kinetic parameters, k_{cat} and k_{cat}/K_m obtained from each plot at different pH values were plotted as a function of pH to Eqs. (10) and (11) describing double and single ionization(s), respectively.

$$y = c/\{1 + ([H]/K_1) + (K_2/[H])\} \tag{10}$$

$$y = c/\{(1 + K_2/[H])\} \tag{11}$$

where y is the pH dependent parameter, c is the pH independent value of the parameter, [H] is the hydrogen ion concentration and K_1 and K_2 are the ionization constants for the ionizable groups involved in catalysis. pH of the assay mixture was adjusted with 50 mM potassium phosphate buffer and temperature kept constant at 25 °C.

2.12. Homology modeling of PfASL

The sequences of ASL from *P. falciparum* (AAC32788), *Plasmodium vivax* (AAL60072), *E. coli* (BAA35953), *Bacillus subtilis* (NP_388526) and *Homo sapiens* (AAC60603) were downloaded from the non-redundant database at NCBI. Multiple sequence alignments were generated using CLUSTALW [26]. The coordinate files for the structures of *E. coli* ASL (PDB code: 2ptr) and *P. vivax* ASL (PDB code: 2qga) were downloaded from Protein Data Bank (http://www.rcsb.org). Homology models of PfASL were generated, using *E. coli* ASL structure liganded to SAMP (PDB code: 2ptr) and *P. vivax* ASL (PDB code: 2qga) (data not shown) as templates, using MODELLER 9v4 [27]. The stereochemical quality of the models was verified using WHAT IF [28] and Verify3D [29]. Molecular visualization and structure analysis was done by PyMOL (DeLano Scientific).

2.13. Parasite growth assays

The 3D7 strain of *P. falciparum* was cultivated *in vitro* using the method described by Trager and Jensen [30]. Parasites were maintained in human O+ erythrocytes isolated from O+ human blood collected from healthy volunteers, at 5% hematocrit in RPMI 1640 (Sigma Chemical Co., St. Louis, USA) containing 10% human serum. AICAriboside was dissolved in water and the compound serially diluted 2-fold over the concentration range 4000–2 μM. Each well contained 250 μl of cell suspension with 2% parasitemia and 2% hematocrit in culture medium. Parasitized and nonparasitized erythrocytes and solvent controls were incorporated in all the tests. The plates were incubated at 37 °C in a candle jar. After 24 h, each well was pulsed with 10 μl of PBS containing 1.0 μCi of [^{3}H] hypoxanthine, and plates were incubated for another 12 h. The contents of each well were then harvested onto glass fiber filters using a Combi-12 automated cell harvester (Molecular Devices, Sunnyvale, CA), washed extensively with distilled water and dried. The incorporated radioactivity was measured as disintegrations per minute using a Wallac 1409 liquid scintillation counter (Wallac Oy, Turku, Finland). The experiments were done in duplicate and repeated twice. For drug treated cultures the percent radioactivity incorporated with respect to the control was plotted against the logarithm of the drug concentration. The concentration causing 50% inhibition of radioisotope incorporation (IC_{50}) was determined by interpolation. A parallel experiment by microscopy, using Giemsa-stained smears, was also conducted.

3. Results

3.1. Biochemical characterization of PfASL

Purified recombinant hexa-histidine tagged PfASL showed a single band on SDS-polyacrylamide gel corresponding to a molecular mass of 55 kDa. MALDI-TOF MS of PfASL gave a molecular mass of 56235 ±56 Da with the expected mass being 56239 Da. Western blotting with monoclonal anti-histidine antibodies further confirmed the identity of recombinant PfASL. The quaternary structure of PfASL was examined using a pre-calibrated Sephacryl S-300 column at 25 °C. The enzyme eluted as a tetramer and no shift in the oligomeric status was seen on varying protein concentration from 20 μM to 5 μM (Fig. 2) or on addition of 1 M NaCl. *P. vivax* ASL in the crystal structure (PDB code 2qga) was found to exist as a tetramer [31]. Previously, ASLs from *B. subtilis* [32], human [4] and other members of the superfamily [5–9] have been shown to exist as tetramers. However, *B. subtilis* ASL

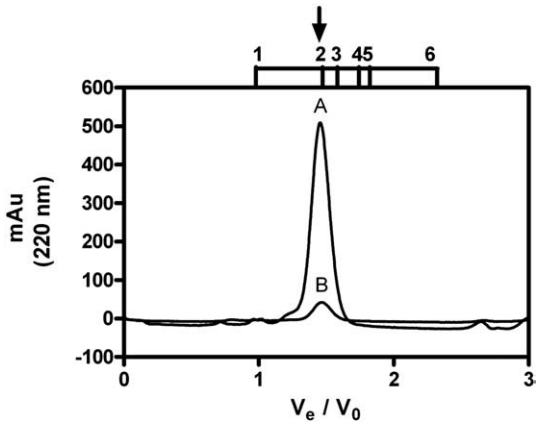

Fig. 2. Oligomeric status of PfASL. Elution profile of PfASL from Sephacryl 300 (S-300) gel filtration column as monitored at 220 nm. V_o or void volume of the column was determined by the use of blue dextran to be 8.0 ml and V_e is the elution volume. Scale above the peak corresponds to the elution of the molecular weight markers and the arrow corresponds to the elution of PfASL. Molecular weight markers are: 1. apoferritin, 440 kDa; 2. amylase, 200 kDa; 3.alcohol dehydrogenase, 150 kDa; 4. bovine serum albumin, 66 kDa; 5. carbonic anhydrase, 29 kDa and 6. cytochrome C, 12.4 kDa. PfASL loaded onto the column was eluted with a buffer containing 50 mM sodium phosphate, pH 7.0, and 150 mM NaCl. The flow rate of the buffer was maintained at 0.5 ml min^{-1}. PfASL concentrations examined were 1 (A) and 0.25 (B) mg ml^{-1} (20 and 5 μM).

Table 1
Kinetic parameters of PfASL for SAMP cleavage and formation

Substrate	K_m (μM)	k_{cat} (s^{-1})
SAMP	32.0±1.7	7.5±0.7
AMP	34.0±1.6	2.9±0.4
Fumarate	760±70	2.9±0.4

All enzyme assays were done at 25 °C in 50 mM potassium phosphate, pH 7.4. Enzyme activity was monitored as a time dependent decrease (SAMP breakdown) or increase (SAMP formation) in absorbance at 290 nm and calculated using a difference extinction coefficient of 4.05 mM^{-1} cm^{-1}. Values reported were obtained from the fit of the data to Eq. (1). Assays were done with three different batches of PfASL with each data point being measured in duplicates.

showed temperature dependence in its oligomeric status with dissociation of the tetramer seen at lower temperatures [33]. PfASL readily catalyzed the reversible breakdown of SAMP with the forward reaction liberating AMP and fumarate and the reverse reaction catalyzing their condensation. Summarized in Table 1 are the kinetic parameters of the forward and reverse reactions. PfASL exhibited similar, low K_m values for SAMP and AMP and a high K_m for fumarate. The k_{cat} value for the forward reaction catalyzed by PfASL was 3 times greater than that for the reverse reaction.

Kinetic mechanism of PfASL was elucidated by steady state initial velocity kinetics in the direction of SAMP formation and, product inhibition and transient kinetics in the direction of SAMP breakdown.

3.2. Initial velocity kinetics

Fig. 3 summarizes results of initial velocity measurements of PfASL catalyzed AMP reaction with fumarate. Initial velocity plots for Bi-Uni reactions following either rapid equilibrium random or steady-state ordered kinetic mechanism, yield line patterns intersecting in the

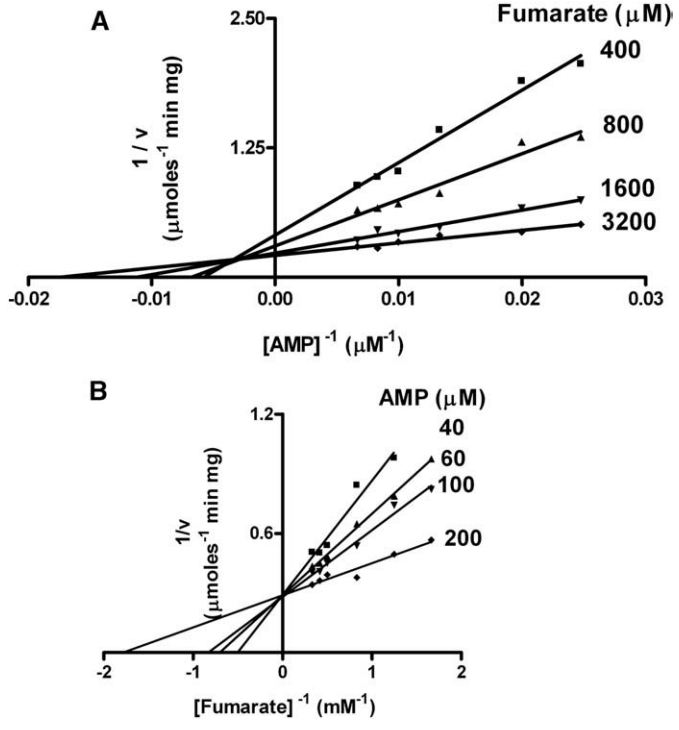

Fig. 3. Initial velocity kinetics of PfASL in the direction of SAMP formation from AMP and fumarate. Each plot corresponds to the activity of PfASL in the direction of SAMP formation with (A) AMP varying at different fixed concentrations of fumarate and (B) fumarate varying at different fixed concentrations of AMP. Each line is a theoretical line based on curve fitting. All assays were done at 25 °C in 50 mM potassium phosphate, pH 7.4. AMP and fumarate were kept at sub-saturating concentrations with the maximum of each being maintained at around five times the respective K_m values.

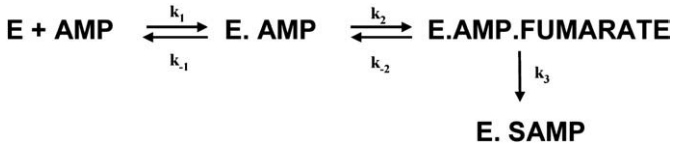

Scheme I.

second quadrant for both substrates [23]. Reciprocal plot of velocities with fumarate varying (0.6–3.0 mM) at different fixed concentrations of AMP (40–200 μM) show convergence on the 1/v axis. This pattern of intersection in a Bi-Uni system supports a rapid equilibrium ordered kinetic mechanism. The linear nature of the reciprocal plots also rules out steady-state random mechanism. Fit of the data to non-linear equations describing the different models for a Bi-Uni system indicated that the preferred model is rapid equilibrium ordered, thereby supporting the inference from the double reciprocal plots. A global fit of the data to the non-linear equations (Eqs. (5) and (6)) describing a rapid equilibrium ordered kinetic model as shown in Scheme I yielded the values 0.3±0.15 mM and 0.5±0.02 mM for K_a (k_{-1}/k_1) and K_b (k_{-2}/k_2), respectively.

3.3. Product inhibition studies

The effect of products, AMP and fumarate, on the rate of SAMP cleavage was determined in order to validate the kinetic mechanism. Reciprocal plot of velocities versus SAMP concentrations at different fixed AMP (0–200 μM) concentrations gave an intersection on the vertical axis indicative of a competitive inhibition (Fig. 4A). Data were also fitted to equation for competitive inhibition (Eq. (2)) to obtain a K_i value of 93±8 μM. The reciprocal plot of velocities with the same range

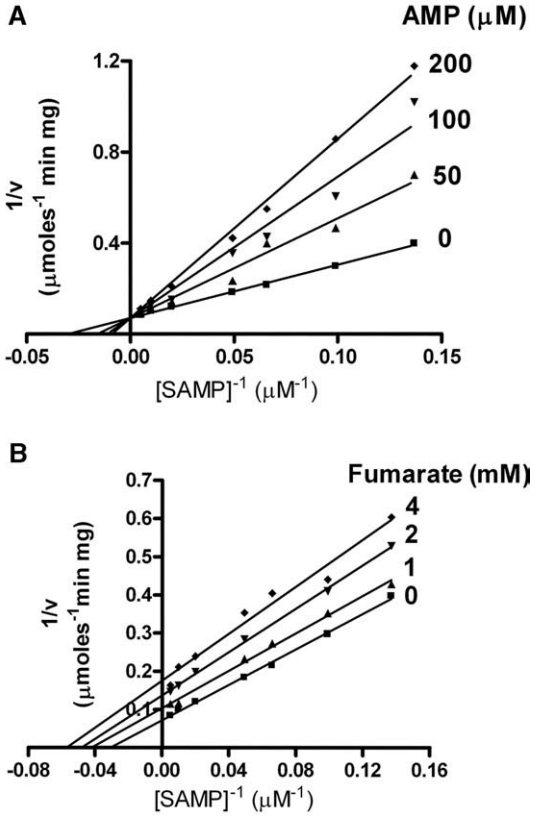

Fig. 4. Product inhibition of PfASL in the direction of SAMP breakdown to AMP and fumarate. PfASL activity was measured at varying SAMP concentrations and at different fixed concentrations of (A) AMP and (B) fumarate. Each line is a theoretical line based on curve fitting. All assays were done at 25 °C in 50 mM potassium phosphate, pH 7.4.

of SAMP concentrations at different fixed fumarate (0–4 mM) concentrations gave a set of lines that intersect in the third quadrant (Fig. 4B). This is typical of noncompetitive inhibition that was further confirmed by comparing non-linear fits of the data to non-competitive (Eq. (3)) and uncompetitive (Eq. (4)) inhibition models. Best fit was obtained for non-competitive model with a K_i value of 3.7±0.2 mM thereby showing that fumarate can bind to both the free and bound forms of the enzyme. However, the high K_{is} (11.7 mM) value as compared to K_{ii} (2.9 mM) indicates that the affinity of fumarate is high for the AMP bound form of enzyme as compared to the free form. Thus, initial velocity and product inhibition studies indicate that PfASL follows a rapid equilibrium ordered bi-uni mechanism in the reverse direction in which AMP binds first to the enzyme followed by fumarate.

3.4. Transient kinetics

Multiple turnover experiment with SAMP being held in excess (100 μM) over the enzyme (5 μM) was done in the direction of SAMP cleavage in order to probe the rate-limiting step in catalysis. Under steady state conditions, PfASL catalyzes 7 turnovers in a second (Table 1). Hence, to monitor the first turnover, we measured the reaction in the millisecond time scale with a stopped flow device attached to a spectrophotometer. The reaction trace did not show any burst (Fig. 5A) and the plot of turnovers with respect to time was linear (Fig. 5C). A catalytic rate of 4.0±0.03 s^{-1} was obtained. The same batch of enzyme was assayed at a concentration of 70 nM with substrate being held at 100 μM under steady state conditions (Fig. 5B). A similar catalytic rate of 6.5±0.03 s^{-1} was obtained from the plot of turnovers versus time (Fig. 5D).

3.5. Primary kinetic isotope effect

ASL catalysis involves the cleavage of two chemically distinct bonds. The first bond to be cleaved is the C(β)–H bond of the succinyl group followed by the C (γ)–N bond joining the succinyl group to the adenylate portion of SAMP. In order to determine which of these two bond cleavages is slower, PfASL activity was compared across two substrates, SAMP and ^{2}H-SAMP. In the latter, the succinyl C–H bond is replaced by a C–D bond. As can be seen from Table 2, the primary kinetic isotope effect (KIE), defined as the ratio of the kinetic parameters, k_{cat} or k_{cat}/K_m for SAMP and [^{2}H]-SAMP, is only 1.3 at pH 7.4. An isotope effect of 3–8 is expected for reactions that follow E2 elimination, if protium is replaced by deuterium and the removal of a hydron is rate limiting [34]. However, it has been debated earlier that KIE values lower than 2 are also possible [35]. This occurs when more than one step determines the rate in the overall reaction. To rule out this possibility, we checked the variation of KIE with respect to pH. The KIE showed only a minor variation from 0.8 at pH 6.6 to 1.4 at pH 8.2 (Table 2). If more than one step would be rate determining, then it is highly unlikely that the activation energies for the different energy maxima in the reaction coordinate are affected equally by pH and hence, produce a constant KIE. Thus, we conclude that C–H bond cleavage occurs rapidly and it is the C–N bond cleavage that determines the overall rate in PfASL catalysis.

Table 2
Primary kinetic isotope effects for the conversion of SAMP to AMP catalyzed by PfASL[a]

pH	($^Dk_{cat}$)[b]	($^Dk_{cat}/K_m$)[c]
6.6	0.8	0.95
7.4	1.3	0.7
7.8	1.6	1.4
8.2	1.4	0.9

[a] PfASL activity was monitored with varying concentrations of SAMP and [^{2}H]-SAMP at 25 °C in 50 mM potassium phosphate buffer at different pH values. Values reported were obtained from the fit of the data to Eq. (1).
[b] $^Dk_{cat}$ is defined as (^{1}H SAMP k_{cat})/(^{2}H SAMP k_{cat}).
[c] $^Dk_{cat}/K_m$ is defined as (^{1}H SAMP k_{cat}/K_m)/(^{2}H SAMP k_{cat}/K_m).

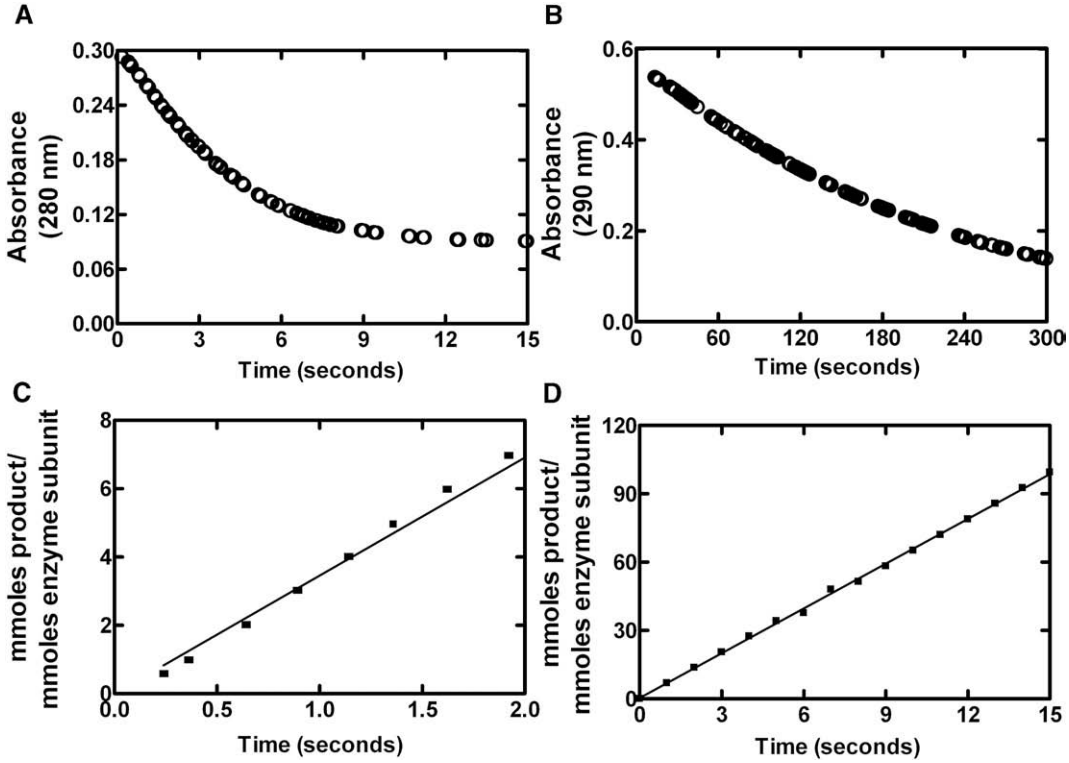

Fig. 5. Transient and steady state kinetics of PfASL in the direction of SAMP breakdown. (A) Reaction trace of SAMP disappearance with respect to time as monitored at 280 nm. Final reaction volume of 300 μl contained 100 μM SAMP, 5 μM PfASL and 50 mM potassium phosphate, pH 7.4 and the reaction was carried out at 25 °C. (B) Reaction trace showing SAMP disappearance with respect to time as monitored at 290 nm. Final reaction volume of 250 μl contained 100 μM SAMP, 73 nM PfASL and 50 mM potassium phosphate, pH 7.4. (C) and (D) Turnovers, defined as mmole product formed per mmole PfASL subunit plotted with respect to time, are shown in the lower panels.

3.6. Solvent isotope effects and proton inventory

Solvent isotope effects were studied to probe the transfer of the proton(s) (to the leaving group nitrogen) as being involved in a rate-limiting step in catalysis. Plot of velocity data in either H_2O or D_2O with varying SAMP concentrations is shown in Fig. 6A. The solvent isotope effect values were obtained as ${}^{D}k_{cat}$ of 1.8±0.3 and ${}^{D}k_{cat}/K_m$ of 1.02±0.5, where ${}^{D}k_{cat}$ and ${}^{D}k_{cat}/K_m$ represent the ratios, k_{cat} in H_2O/k_{cat} in D_2O and (k_{cat}/K_m) in $H_2O/(k_{cat}/K_m)$ in D_2O, respectively. PfASL activity measured in different fractional concentrations of D_2O compared with 100% D_2O gave a straight line (Fig. 6B) indicating that a single proton is transferred in the slowest step of the entire reaction [25]. Data was fitted to Eq. (7) to obtain the deuterium fractionation factor $\phi^T=0.7$ and ${}^{D}k$, the solvent deuterium isotope effect, of 1.5.

3.7. Effect of pH on PfASL catalysis

The effect of pH on PfASL kinetic parameters, k_{cat} and k_{cat}/K_m, for the cleavage of SAMP to AMP and fumarate was monitored over a pH range of 6.0 to 9.0. k_{cat} is a first order rate constant and its variation with pH describes the ionization processes taking place in the catalytic complex. On the other hand, k_{cat}/K_m is a second order rate constant that describes the ionization(s) of either the free substrate or the free enzyme towards the catalytic complex formation. Pre-incubation of the enzyme in different pH buffers (6.0–9.0) did not cause any irreversible loss in activity. Hence, the

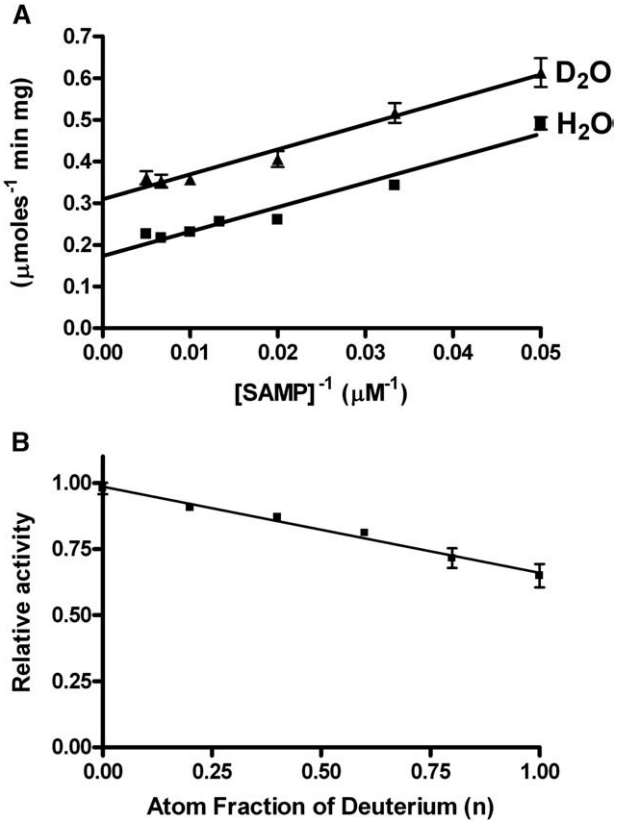

Fig. 6. Solvent deuterium kinetic isotope effect and proton inventory. (A) PfASL activity was determined with varying SAMP concentrations in either H_2O or D_2O. PfASL activity was monitored in 50 mM potassium phosphate buffer, pH 7.4 (prepared either in H_2O or D_2O) with varying SAMP concentrations. Data were fitted by linear regression using GraphPad prism Software, version 4.0 (GraphPad Software, Inc., San Diego, CA). (B) PfASL activity (monitored at a saturating SAMP concentration of 200 μM) as a function of mole fraction of D_2O. Data were fitted to the Gross–Butler equation describing a linear proton inventory (Eq. (7)).

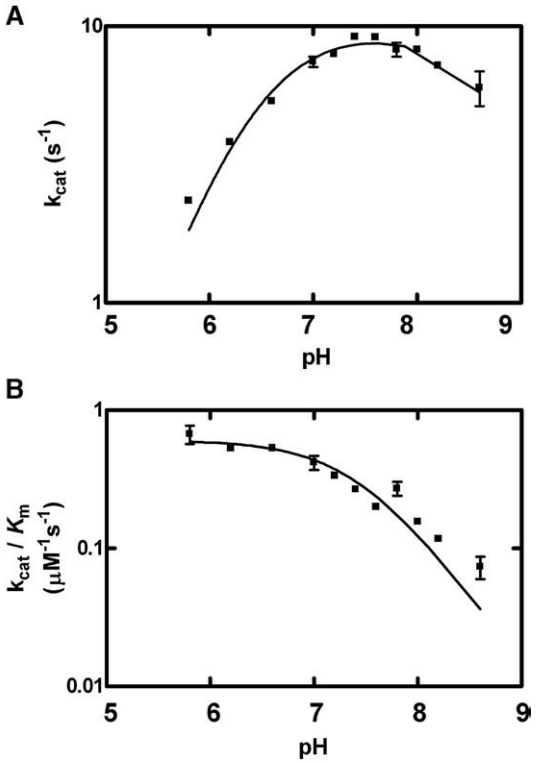

Fig. 7. pH kinetics. PfASL activity was determined at different concentrations of SAMP over a range of pH values (5.8–8.8). Data at each pH value was fitted to Eq. (1) to obtain the kinetic parameters, k_{cat} and k_{cat}/K_m. Data were fit to equations that describe either a double ionization process (A) (Eq. (10)) or a single ionization process (B) (Eq. (11)). Each line is a theoretical line based on curve fitting. pH was maintained at the desired value using 50 mM potassium phosphate buffer in a final reaction volume of 250 μl.

inflections observed in the pH profile can be approximated to the true ionizations of the enzyme's catalytic groups. The plot of k_{cat} versus pH was obtained as a bell shaped curve with both the acidic and the alkaline limbs (Fig. 7A). The apparent pKa values, pK_1 of 6.45±0.02 and pK_2 of 8.73±0.01, were obtained by fitting the data to Eq. (10) describing a double ionization process. In contrast to the k_{cat} profile, the k_{cat}/K_m profile exhibited only the alkaline limb (Fig. 7B). Data were fitted to Eq. (11) describing a single ionization process to obtain a pK value of 7.4±0.05. This ionization could be occurring in either the free substrate or free enzyme. The possibility of the former could be ruled out as the spectral properties of SAMP [36] do not highlight any ionization (other than the secondary phosphate ionization at pH 6.7) taking place in the pH range studied here. Hence, it can be inferred that this ionization is taking place in the free enzyme. From both these profiles, the implication is that the group corresponding to pK_1, which acts as a catalytic base at the optimum pH, gets ionized only in the catalytic complex but not in the free enzyme. This in turn indicates that the substrate, SAMP assists in this ionization. On the other hand, the group corresponding to pK_2 shows a significant change in its pK_a value, from 7.4 to 8.73, when the enzyme binds the substrate.

3.8. Activity of Ser298 mutants

It has been shown in *E. coli* ASL that a conserved serine, S295, may act as the catalytic base [13] due to its proximity to the C(β)–H group of the substrate. Mutation of this residue in *B. subtilis* and *H. sapiens* ASLs results in complete loss of activity [37]. The corresponding serine in PfASL is S298. In order to probe the role of this residue in PfASL catalysis, S298A and S298C mutants were generated. The structural integrity of both the mutants was assessed by circular dichroism and

fluorescence spectroscopy. The wild type and the mutant proteins gave overlapping spectra (data not shown). This indicates that mutation of serine 298 to alanine or cysteine did not lead to gross changes in the structural properties of PfASL. However, the specific activity of S298A mutant at 9.5×10^{-3} μmol $min^{-1}mg^{-1}$ was 1000 fold lower than that of the wild enzyme. Also, the specific activity remained unchanged upon variation of pH. Interestingly, the isosteric mutant S298C showed complete loss of activity. These results indicate the indispensability of this residue to PfASL catalysis.

3.9. SAICAR reaction

Due to the unavailability of SAICAR from any commercial source, we monitored the condensation of AICAR and fumarate to SAICAR in a continuous spectrophotometric assay at 267 nm with enzyme concentration similar to that used for AMP to SAMP conversion. No measurable activity was obtained even on using 10-fold excess of enzyme. However, AICAR competitively inhibited the SAMP breakdown by PfASL with an IC_{50} value of 251±1 μM. Addition of AICAR and fumarate in combination drastically reduced the AICAR IC_{50} to 57±1 μM (data not shown). This suggested a synergistic mode of inhibition and indicated that both AICAR and fumarate together bind PfASL. With this evidence, a large-scale synthesis of SAICAR from AICAR and fumarate was attempted using PfASL. Thin-layer chromatography of the reaction mixture showed the appearance of a new spot that could correspond to SAICAR. Purification of this compound from the reaction mixture was done on DEAE-ion exchange column with a linear gradient of ammonium bicarbonate (pH 8.0). The peak that eluted after AICAR and fumarate was found by MALDI-MS to have a mass of 455±0.4 Da corresponding to the monoprotonated mass of SAICAR (data not shown).

As the sensitivity of the assay for SAICAR reaction was lower than the SAMP reaction, enzyme amount was increased to 1–2 μg to obtain reliable activity measurements. The K_m and k_{cat} values obtained for SAICAR cleavage were 40.0±8 μM and 7.0±0.7 s^{-1}, respectively. However, the kinetic parameters for the reverse reaction (AICAR+fumarate) could not be determined due to the poor sensitivity of the assay.

Table 3
Comparison of the thermodynamic parameters associated with the binding of AMP and AICAR to PfASL[a]

Ligand	Stoichiometry (n)	Dissociation constant ($K_{dissoc.}$) (mM)	Enthalpy change (ΔH^o) (kcal mol^{-1})	Entropy change (ΔS^o) (cal K^{-1} mol^{-1})	Free energy change (ΔG^o)[b] (Kcal mol^{-1})
AMP	1.0	0.17±0.02	−1.8±0.08	10	−5.15
AICAR	1.0	0.17±0.06	−0.75±0.09	14	−5.13

[a] The enzyme was maintained at a concentration of 160 μM and titrated with 5 μl volumes of AMP and AICAR at a constant temperature of 25 °C. The resulting heat changes were recorded on a VP-ITC. The values reported are obtained from the fit of the data in Fig. 8 to the single site binding model using ORIGIN software.
[b] Free energy change (ΔG^o) was calculated from Eq. (8).

3.10. Thermodynamics of binary complex formation

Thermodynamic characterization of the binding of AMP and AICAR to PfASL in the absence of fumarate was carried out by isothermal titration calorimetry. The raw calorimetric signals from the ITC titration were integrated and corrected for the heat of dilution. The resulting enthalpy change was plotted with respect to the molar ratio of ligand and protein as shown in Fig. 8. The associated thermodynamic parameters for the interaction are listed in Table 3. The binding of AMP to PfASL occurred at a single site with weak affinity as indicated by the high value of the dissociation constant ($K_{dissoc.\ AMP}$=170 μM). AICAR also bound PfASL at a single site and with an affinity similar to that of AMP ($K_{dissoc.\ AICAR}$=170 μM). A slightly greater enthalpy change was observed in the interaction of AMP with PfASL. This could imply additional protein-ligand interactions in AMP.PfASL complex that are absent in AICAR.PfASL complex. AICAR has an incomplete purine ring and thus is more flexible than AMP in solution. This inherent flexibility could explain the marginal

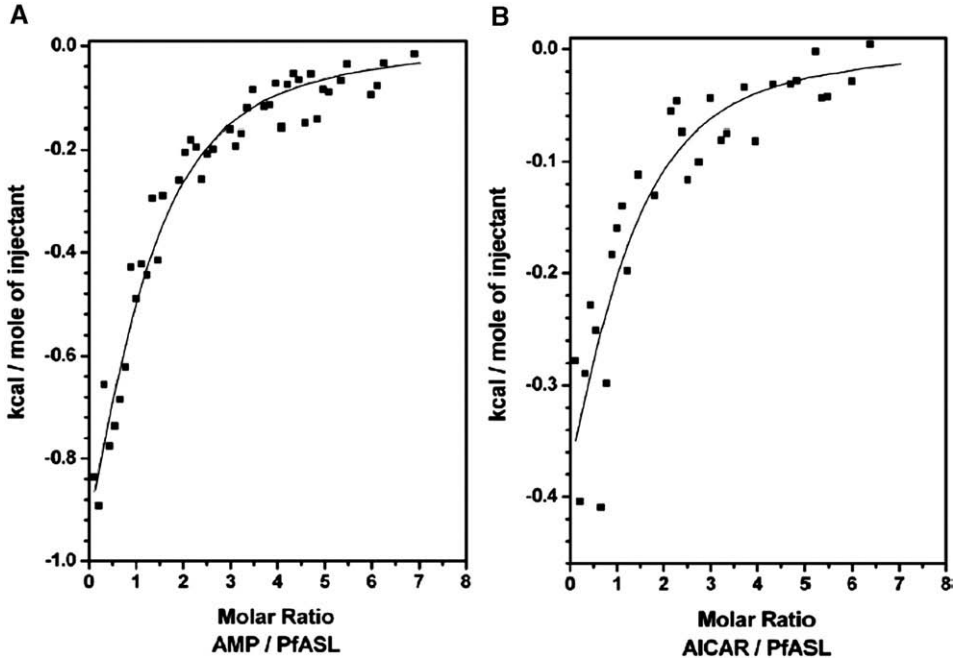

Fig. 8. Thermodynamic characterization of the interaction of PfASL with AMP. PfASL (160 μM) was titrated with 5 μl volumes of AMP (A) or AICAR (B) each at 5 mM stock concentration in 50 mM potassium phosphate, pH 7.4 containing 100 mM NaCl and 10% glycerol, at 25 °C. The raw calorimetric signals from the ITC titration were integrated and corrected for the heat of dilution. The resulting enthalpy change was plotted with respect to the molar ratio of ligand and protein. Data were fitted to the single site binding model (using the software ORIGIN) after correction for the heat of dilution of ligand.

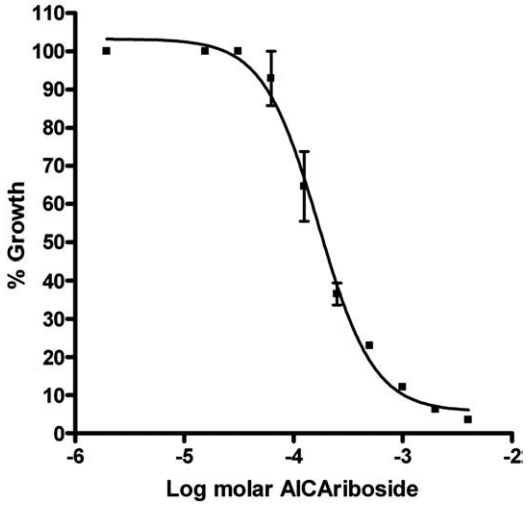

Fig. 9. Effect of AICAriboside on uptake of [^{3}H] hypoxanthine by parasitized erythrocytes in culture. Culture was treated with AICAriboside for 24 h, followed by the addition of 1 μCi [^{3}H] hypoxanthine to each well. The cells were harvested after another 12 h and [^{3}H] hypoxanthine was quantified by scintillation counting. The radioactive counts obtained from culture without the drug were set as 100% growth. The graph represents mean of two independent experiments done in duplicate.

increased entropy change upon binding of AICAR to PfASL. Most importantly, the overall free energy change associated with the binding of these two ligands was similar ($\Delta G^o = -5.1$ kcal mol^{-1}).

3.11. Parasite growth assays

The extended ability of PfASL to bind AICAR prompted us to test the effect of the latter on in vitro parasite growth. We did not see any change in the parasitemia after 24 h of incubation with AICAR in comparison to the control. We then tested the effect of the cell permeable AICAriboside on in vitro parasite growth (as monitored by incorporation of [^{3}H]-hypoxanthine into the genomic DNA). AICAriboside inhibited the parasite growth with half-maximal inhibitory concentration (IC_{50}) of 167±5 μM (Fig. 9). Similar IC_{50} values were obtained by following parasite growth through microscopy.

4. Discussion

We report here a detailed biochemical characterization of PfASL. The only other paper that talks about the kinetic aspect(s) of ASL is that by Bridger and Cohen published in 1968 [10]. This was the first report that discussed mainly on the order of product release and aspects relating to rate limiting step(s) have not been enunciated. In fact, they assumed the rate-limiting step to be other than the cleavage of C–H and C–N bonds. ASL catalysis in the forward direction of SAMP breakdown to AMP and fumarate involves the cleavage of two distinct chemical bonds, the C(β)–H bond of the succinyl group followed by the C(γ)–N bond joining the succinyl group to the adenylate portion in SAMP.

The value of K_a (k_{-1}/k_1 in Scheme I) as monitored by initial velocity kinetics and verified by equilibrium binding measurements by isothermal calorimetry ($K_{dissoc.}$) (0.3±0.15 mM and 0.17±0.02 mM, respectively) was significantly higher than the K_m value for AMP (34.0±1.6 μM). The lower K_m value indicates an increased affinity of AMP towards the enzyme under conditions of catalysis. This is possible only if the three different enzyme forms E, E.AMP and E.AMP.FUMARATE exist in a rapid equilibrium as shown in Scheme I. The presence of fumarate shifts the equilibrium towards increased product (SAMP) formation and therefore, increased affinity of AMP to the enzyme. Examination of the double reciprocal plot of 1/v vs 1/fumarate at different fixed concentrations of AMP brings out two kinetic aspects of catalysis by PfASL, (1) the decrease in apparent K_b for fumarate with increase in AMP concentration supports the presence of rapid equilibrium between E.AMP.FUMARATE and FUMARATE and, (2) absence of change in $V_{max.}$ with increase in AMP concentration eliminates rapid equilibrium between E.AMP.FUMARATE and E.SAMP thereby indicating that the process of chemical conversion is rate limiting.

An ordered release of fumarate followed by AMP from PfASL was also validated by product inhibition studies. However, the large difference between the K_{is} (11.7 mM) and K_{ii} (2.3 mM) values for inhibition with fumarate indicates the presence of a minor alternate path in which AMP is released first followed by fumarate.

Our transient kinetic data in the direction of SAMP breakdown reconfirms the model proposed from initial velocity kinetics. The absence of a 'burst' in the reaction trace indicates that the rate limiting step is that of catalysis with step(s) subsequent to it occurring at a faster rate. Moreover, absence of a lag in the reaction trace rules out a steady state step prior to catalysis. Taken together, these results are consistent with a rapid equilibrium Uni-Bi ordered kinetic model with the catalytic step being rate limiting as shown in the Scheme I.

Elimination reactions that result in alkene formation can be of the type E1, E2 or E1cB. E1 elimination involves loss of leaving group leading to the formation of carbocation, which is followed by loss of hydrogen leading to double bond formation [38]. In E2 elimination, the two bond cleavages, C–H and C–X (where X is an electronegative group) take place in a single transition state and hence, a concerted mechanism [39]. The primary KIE values on replacement of C–H with a C–D bond for this mechanism are expected to be in the range of 3–8 [34]. In E1cB reactions a strong base abstracts the α proton generating a carbanion intermediate followed by an electron pair expelling the leaving group in a rate limiting step leading to double bond formation [40]. In this mechanism, only the C–N bond cleavage takes place in the transition state and the KIE on replacement of C–H with a C–D is expected to be unity. Our kinetic data with [^{2}H]-SAMP, where C (β)–H is replaced by a C(β)–D bond, gave a KIE of around unity (Table 2) ruling out both E1 and E2 mechanisms. Further, our solvent deuterium isotope effect and proton inventory data showed that a single proton is transferred in a rate-determining step from the solvent through the enzyme to the reactant. Thus, we conclude from these results that the process of C–N bond cleavage is rate limiting and hence, an E1cB mechanism. Previously, the existence of a carbanion like intermediate in ASL catalysis has been shown indirectly by the tight binding of the nitro analogue of SAMP (a mimic of the carbanion form of SAMP) to the yeast ASL [41]. Our work provides the first direct kinetic evidence for the presence of a carbanion like intermediate in PfASL catalysis. Also, other members of this superfamily of enzymes such as aspartase [42] and arginosuccinate lyase [43] have been reported to catalyze the reaction through a carbanion like transition state intermediate.

The faster cleavage of the C–H bond over the C–N bond in PfASL catalysis is contrary to the expectation. This is because of the poor acidity of the α protons of carboxylate anions. The weak acidity of the α protons of carboxylate anions is because of the poor stability of the resultant carbanion species [44]. The simple strategy for increasing the acidity of these protons would therefore be to increase the stability of the carbanion species. Indeed, enzymes do so by two mechanisms: stabilization by metal ions and stabilization by hydrogen bonds [45]. As metal ions do not play any role in the catalysis by ASL, the stabilization of the carbanion intermediate by hydrogen bonds with groups on the enzyme becomes a possible option. Indeed, Tsai *et al.* [13] highlighted the occurrence of such strong hydrogen bonds in the structure of *E. coli* ASL liganded to SAMP (Protein data bank I.D: 2ptr). T122, S123, S296 and H91 (*E. coli* ASL numbering) are the residues involved in hydrogen bonding with the α-carboxylate group of SAMP and hence, aid in the stabilization of the carbanion intermediate. Similar interactions must be operating in PfASL also as all the implicated residues are conserved across the two enzymes.

pH kinetics shows the ionization of the catalytic base only in the enzyme substrate complex highlighting the probable role of the substrate in facilitating this process. Previously, His 141 in *B. subtilis* ASL was proposed to be the catalytic base, a conclusion arrived at from both site directed mutagenesis and site-specific modification studies [11]. However, the corresponding His171A mutant *E. coli* ASL structure liganded with SAMP shows a serine (S295) in proximity to the C(β)–H bond of the substrate [13]. This serine lies in a highly conserved flexible loop, which closes over the active site upon substrate binding. Due to the proximity of serine hydroxyl to the C(β)–H of the substrate, this residue has been suggested to act as a putative catalytic base in the conversion of SAMP to AMP and fumarate [13]. The corresponding serine in PfASL is S298. A 1000 fold drop in specific activity in the S298A point mutant validated the indispensable role of this residue in PfASL catalysis. Moreover, the specific activity of S298A mutant remained unchanged upon variation of pH, thereby implicating the direct role of this residue in PfASL catalysis, probably as a base as in the case of *E. coli* ASL. The presence of poor residual activity in S298A mutant could possibly arise from the binding of the substrate to a highly structured active site environment favorable enough for proton abstraction. In order to examine whether the thiol from cysteine can replace serine hydroxyl in PfASL catalysis, S298C mutant was generated. However, the mutant displayed a complete loss of activity indicating (1) a preferential requirement for a hydroxyl as compared to a thiol for proton abstraction and/or (2) disruption of the active site environment because of geometric and electrostatic perturbations on substitution of a poorly reactive hydroxyl with a highly reactive thiol group.

Serine can function as a catalytic base only if its side chain –OH is ionized to form an oxyanion species, which being a very strong nucleophile can easily abstract a proton. As the pK_a of the β-OH group of serine is around 15, its ionization at the physiological pH becomes likely only in the presence of a neighboring basic group. However, no obvious groups on the enzyme, which could serve to abstract the hydroxyl proton of serine, were detected in the structure of *E. coli* ASL complexed to SAMP other than the backbone amide nitrogens of T297 and M298 [13]. It is well known that the electrons on the nitrogen atom in a peptide bond –C(O)–NH– are not freely available for reactivity as they are involved in the resonance stabilization of the peptide unit. Hence, the poor nucleophilicity of the peptide amide group makes it a bad candidate for the abstraction of the proton from serine hydroxyl group.

Interestingly, our pH kinetics studies with PfASL indicate a possible assistance of the substrate in the ionization of the catalytic base, S298 (Fig. 7). A closer examination of the liganded *E. coli* ASL structure highlighted the presence of the alpha carboxylate oxygens of SAMP in close proximity to the serine hydroxyl (3.8 Å) with a network of hydrogen bonds from the latter through the substrate and into the functional groups in the protein (Fig. 10A). The extensive hydrogen-bonding network of the enzyme residues with the substrate α-carboxylic group could be expected to serve two purposes: (a) to stabilize the carbanion intermediate and (b) to serve as a probable sink for the proton abstracted by the substrate carboxylic group from serine 295. Alignment of the catalytic loop residues 280-310 of ASL sequences from *E. coli*, *P. falciparum*, *P. vivax*, *B. subtilis* and *H. sapiens* (Fig. 10B) indicate a higher homology of both the plasmodial enzymes to this region in the *E. coli* ASL. Modelling of the *P. falciparum* structure on the *E. coli* enzyme led to a modeled loop orientation similar to that seen in *E. coli* structure with serine 298 in close proximity to C(β)–H of SAMP (Fig. 10C). However, modelling of PfASL structure on the available *P. vivax* ASL structure (Protein data bank code: 2qga) in which the catalytic loop has not been mapped led to a modeled loop in an orientation different from that seen in the *E. coli* ASL structure (data not shown). These differences in loop conformation observed in the two modeled structures of PfASL emphasize the high mobility of the loop.

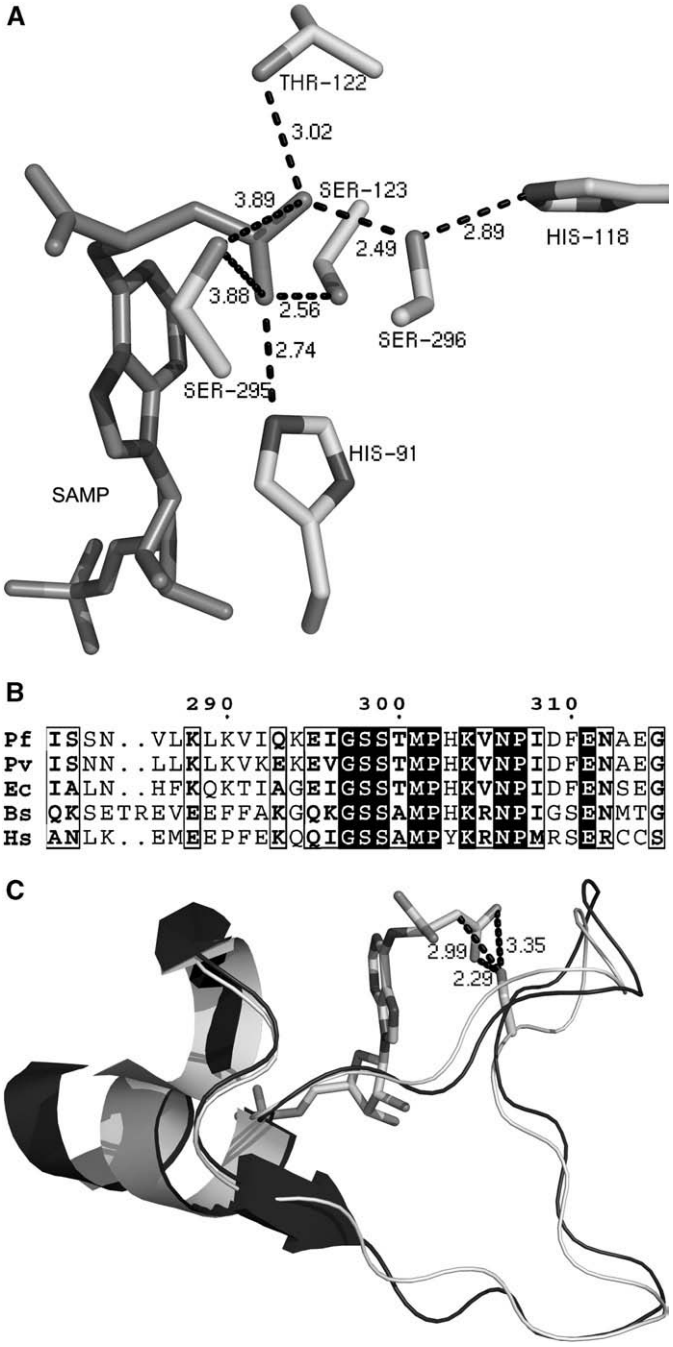

Fig. 10. The catalytic loop and the environment of the catalytic serine in adenylosuccinate lyase. (A) Hydrogen bonding network originating from Ser295 in *E. coli* ASL. Only the side chains are shown for clarity. Dotted lines represent hydrogen bonds and numbers correspond to the interatomic distances in angstrom (Å). (B) Multiple sequence alignment of the catalytic loop residues in ASL. Ec, *E. coli* ASL; Pf, *P. falciparum* ASL; Bs, *B. subtilis* ASL and Hs, *H. sapiens* ASL. Alignment was generated using CLUSTALW [26]. The numbers above the sequences indicate the residue numbering in PfASL sequence (C) Structural superposition of the catalytic loop of modeled PfASL (light) and *E. coli* ASL (dark) (2ptr). Also shown in the model structure of PfASL are the contacts of the side chain hydroxyl of the putative catalytic base Ser 298 with the C (β)–H of SAMP (2.99 Å) and the carboxylate oxygens of SAMP (2.29 Å and 3.35 Å respectively). Modelling of PfASL was done as described in the materials and methods using MODELLER 9v4 with *E. coli* ASL as a template. The figure was generated using PyMol v0.99 (DeLano Scientific).

Thus, in PfASL catalysis, generation of the oxyanion of Ser298 by the SAMP carboxylic groups could be the mechanism involved in priming S298 C(β)-OH to facilitate proton abstraction as shown in Fig. 11. This is also supported by the observation that the group

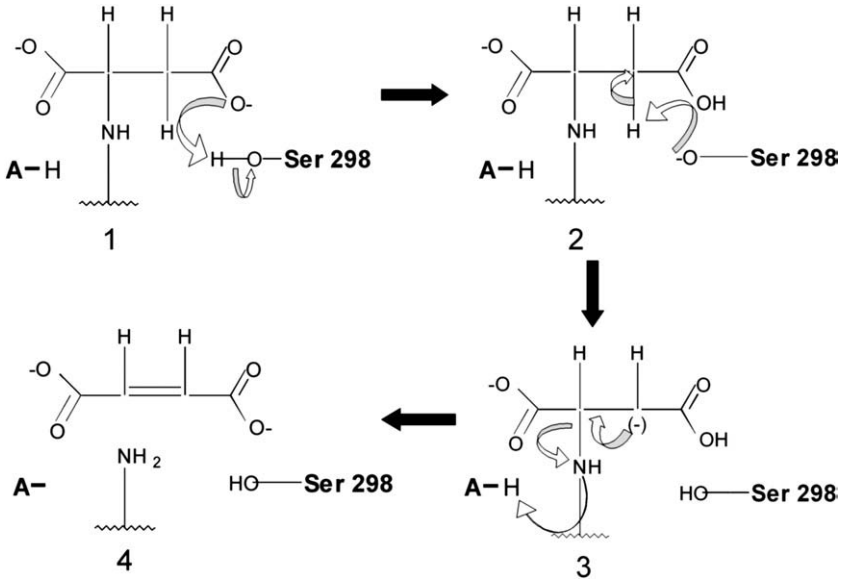

Fig. 11. Catalytic scheme for PfASL.

corresponding to pK_1 in *B. subtilis* ASL has been proposed to be a free acid [46] that could be either a phosphate or a carboxylic group. However, whether the phenomenon of substrate dependent base ionization seen in PfASL hold true for other ASLs is not clear. An important aspect is the variation seen in the behavior of kinetic parameters with respect to pH for ASLs from different species. *E. coli* ASL, for example, shows a 3–5 fold higher activity at pH 8.5 than at a pH value of 7.4 [13], while ASLs from *B. subtilis* [2] and *H. sapiens* [4] show optimum activity at pH 7.4. A second difference is the bell shaped curve seen in the k_{cat}/K_m vs pH profile in the human ASL [4]. Finally, the model of the missing signature loop in ASL structures from *B. subtilis* and *H. sapiens* showed dramatic variations in the orientation of the loop [37]. These variations may reflect the true differences across ASLs from different organisms.

ASLs from *B. subtilis* [2], *N. crassa* [3], and *H. sapiens* [4] have been shown to catalyze the SAICAR and SAMP cleavage with equal efficiency. This could be a consequence of the nature of interaction of ASLs with the ligands, indicating that fully active ASLs do not selectively loose one activity while retaining the other. However, in some of the human ASL mutants, the binding of SAMP to ASL is impaired to a greater extent than that of SAICAR showing that certain changes in the enzyme's primary sequence do lead to differential effects on the two substrates [47,48]. Our results show that PfASL catalyzes both the cleavage reactions of SAMP and SAICAR with the same efficiency. Also, the enzyme makes no significant distinction in binding AICAR and AMP to form the binary complex.

The significance of the retention of SAICAR activity in PfASL is not clear as the subsequent enzyme for the metabolism of AICAR, AICAR transformylase (E.C. number 2.1.2.3), is absent in the *P. falciparum* genome [14]. In organisms that have a functional *de novo* purine biosynthetic pathway, AICAR transformylase converts AICAR to IMP. Thus, in *P. falciparum* AICAR represents a 'non-utilizable metabolic block' and hence, can be used as a novel putative anti-malarial. In support of this, we saw a dose dependent inhibition of parasite growth with the cell permeable AICAriboside (Fig. 8). AICAriboside gets phosphorylated by adenosine kinase to AICAR in mammalian cells, [49,50], thereby activating an AMP-activated protein kinase [51]. It has been shown that the cytotoxic effect of AICAriboside is mediated through AMP-activated protein kinase [52]. No annotations for either of these two kinases exist in the Plasmodium genome database, PlasmoDB [53]. Thus, we hypothesize that AICAriboside probably gets phosphorylated to AICAribotide by a parasite encoded 5′ purine nucleotidase (PFL0305c) [54]. Purine nucleotidases have recently been shown to also have a phosphotransferase activity [55] in which the phosphate group is transferred from a nucleoside monophosphate to another nucleoside. AICAribotide, thus formed, may compete with SAMP for PfASL active site thereby bringing about its inhibition. Though studies using AICAriboside suggest a cytotoxic effect on mammalian cells [52], comparative analysis at concentrations that kill the parasite is needed to validate this molecule as a potential anti-parasitic agent.

5. Conclusions

In conclusion, our studies for the first time highlight the biochemical, kinetic and catalytic features of ASL from a parasitic protozoan, *P. falciparum*. The enzyme follows a rapid equilibrium uni-bi ordered kinetic mechanism in the reversible cleavage of SAMP to AMP and fumarate. Catalysis proceeds through a 'carbanion' transition state as the overall rate is dictated by the C–N bond cleavage in the substrate. The carboxylic group of the substrate probably activates the catalytic base for attack on its C(β)–H bond. Finally, the enzyme also acts on SAICAR with similar kinetic and thermodynamic properties as on SAMP. Due to the extended substrate specificity of PfASL, we propose that AICAR or its analogues that have no role to play in parasite metabolism can act as leads for development of novel anti-malarials.

Acknowledgements

We thank Prof. Raghavan Varadarajan, Molecular Biophysics Unit, Indian Institute of Science, Bangalore for permitting us the use of VP-ITC machine, Prof. Jayant B. Udgaonkar, National Centre for Biological Sciences, Bangalore for permitting access to the SFM 4.0 Biologic Stopped Flow Apparatus and Dr. Srinivasa Rao Raghothoma, NMR research centre, Indian Institute of Science for NMR measurements. This study was funded by grants from CSIR and CSIR-NMITLI, Government of India. VB. is a recipient of CSIR-UGC senior research fellowship. BS. is a recipient of CSIR senior research fellowship.

References

[1] S. Ratner, In: P.D. Boyer (Ed.), 3rd ed., The Enzymes, Vol.7, Academic Press, New York, 1972, pp. 167–197.

[2] J.B. Palenchar, J.M. Crocco, R.F. Colman, The characterization of mutant *Bacillus subtilis* adenylosuccinate lyases corresponding to severe human adenylosuccinate lyase deficiencies, Protein Sci. 12 (2003) 1694–1705.
[3] N.H. Giles, C.W. Partridge, N.J. Nelson, The genetic control of adenylosuccinase in *Neurospora crassa*, Proc. Natl. Acad. Sci. U. S. A. 43 (1957) 305–317.
[4] R.L. Stone, H. Zalkin, J.E. Dixon, Expression, purification, and kinetic characterization of recombinant human adenylosuccinate lyase, J. Biol. Chem. 268 (1993) 19710–19716.
[5] E.A. Toth, T.O. Yeates, The structure of adenylosuccinate lyase, an enzyme with dual activity in the de novo purine biosynthetic pathway, Structure 8 (2000) 163–174.
[6] T.M. Weaver, D.G. Levitt, M.I. Donnelly, P.P. Stevens Wilkens, L.J. Banaszak, The multisubunit active site of fumarase C from *Escherichia coli*, Nat. Struct. Biol. 2 (1995) 654–662.
[7] A. Simpson, O. Bateman, H. Driessen, P. Lindley, D. Moss, S. Mylvaganam, E. Narebor, C. Slingsby, The structure of avian eye lens-crystallin reveals a new fold for a superfamily of oligomeric enzymes, Nat. Struct. Biol. 1 (1994) 724–733.
[8] W. Shi, J. Dunbar, M.M. Jayasekera, R.E. Viola, G.K. Farber, The structure of L-aspartate ammonia-lyase from *Escherichia coli*, Biochemistry 36 (1997) 9136–9144.
[9] M.A. Turner, A. Simpson, R.R. McInnes, P.L. Howell, Human argininosuccinate lyase: a structural basis for intragenic complementation, Proc. Natl. Acad. Sci. U. S. A. 94 (1997) 9063–9068.
[10] W.A. Bridger, L.H. Cohen, The kinetics of adenylosuccinate lyase, J. Biol. Chem. 243 (1968) 644–650.
[11] T.T. Lee, C. Worby, J.E. Dixon, R.F. Colman, Identification of His^{141} in the active site of *Bacillus subtilis* adenylosuccinate lyase by affinity labeling with 6-(4-Bromo2,3 dioxobutyl)thioadenosine 5-monophosphate, J. Biol. Chem. 272 (1997) 458–465.
[12] T.T. Lee, C. Worby, Z.Q. Bao, J.E. Dixon, R.F. Colman, His^{68} and His^{141} are critical contributors to the intersubunit catalytic site of adenylosuccinate lyase of *Bacillus subtilis*, Biochemistry 37 (1998) 8481–8489.
[13] M. Tsai, J. Koo, P. Yip, R.F. Colman, M.L. Segall, P.L. Howell, Substrate and product complexes of *Escherichia coli* adenylosuccinate lyase provide new insights into the enzymatic mechanism, J. Mol. Biol. 370 (2007) 541–554.
[14] M.J. Gardner, N. Hall, E. Fung, O. White, M. Berriman, R.W. Hyman, J.M. Carlton, A. Pain, K.E. Nelson, S. Bowman, I.T. Paulsen, K. James, J.A. Eisen, K. Rutherford, S.L. Salzberg, A. Craig, S. Kyes, M.S. Chan, V. Nene, S.J. Shallom, B. Suh, J. Peterson, S. Angiuoli, M. Pertea, J. Allen, J. Selengut, D. Haft, M.W. Mather, A.B. Vaidya, D.M. Martin, A.H. Fairlamb, M.J. Fraunholz, D.S. Roos, S.A. Ralph, G.I. McFadden, L.M. Cummings, G.M. Subramanian, C. Mungall, C.J. Venter, D.J. Carucci, S.L. Hoffman, C. Newbold, R.W. Davis, C.M. Fraser, B. Barrell, Genome sequence of the human malaria parasite *Plasmodium falciparum*, Nature 419 (2002) 498–511.
[15] P. Reyes, P.K. Rathod, D.J. Sanchez, J.E. Mrema, K.H. Rieckmann, H.G. Heidrich, Enzymes of purine and pyrimidine metabolism from the human malaria parasite, *Plasmodium falciparum*, Mol. Biochem. Parasitol. 5 (1982) 275–290.
[16] H.T. Shigeura, C.N. Gordon, The mechanism of action of hadacidin, J. Biol. Chem. 237 (1962) 1937–1940.
[17] H.K. Webster, J.M. Whaun, M.D. Walker, T.L. Bean, Synthesis of adenosine nucleotides from hypoxanthine by human malaria parasites (*Plasmodium falciparum*) in continuous erythrocyte culture: inhibition by hadacidin but not alanosine, Biochem. Pharmacol. 33 (1984) 1555–1557.
[18] V.M. Marshall, R.L. Coppel, Characterisation of the gene encoding adenylosuccinate lyase of *Plasmodium falciparum*, Mol. Biochem. Parasitol. 88 (1997) 237–241.
[19] M.M. Bradford, A rapid and sensitive method for the quantitation of microgram quantities of protein utilizing the principle of protein-dye binding, Anal. Biochem. 72 (1976) 248–254.
[20] A.R. Shenoy, S.S. Visweswariah, Site-directed mutagenesis using a single mutagenic oligonucleotide and DpnI digestion of template DNA, Anal. Biochem. 319 (2003) 335–336.
[21] K. Tornheim, J.M. Lowenstein, The Purine Nucleotide Cycle: the production of ammonia from aspartate by extracts of rat skeletal muscle, J. Biol.Chem. 247 (1972) 162–169.
[22] D.O. Woodward, H.D. Braymer, Purification and properties of *Neurospora* adenylosuccinase, J. Biol. Chem. 241 (1966) 580–587.
[23] I.H. Segel, Enzyme kinetics, Behavior and Analysis of Rapid Equilibrium and Steady-State Enzyme Systems, John Wiley & Sons, Inc., NY, 1975, pp. 320–329.
[24] F. Van den Bergh, M.F. Vincent, J. Jaeken, G. Van den Berghe, Radiochemical assay of adenylosuccinase: demonstration of parallel loss of activity toward both adenylosuccinate and succinylaminoimidazole carbamide ribotide in liver of patients with the enzyme defect, Anal. Biochem. 193 (1991) 287–291.
[25] K.B. Showen, R.L. Showen, Solvent isotope effects of enzyme systems, Methods Enzymol. 87 (1982) 551–606.
[26] D. Higgins, J. Thompson, T. Gibson, J.D. Thompson, D.G. Higgins, T.J. Gibson, CLUSTAL W: improving the sensitivity of progressive multiple sequence alignment through sequence weighting, position-specific gap penalties and weight matrix choice, Nucleic Acids Res 22 (1994) 4673–4680.
[27] A. Sali, T.L. Blundell, Comparative protein modelling by satisfaction of spatial restraints, J. Mol. Biol. 234 (1993) 779–815.
[28] G. Vriend, WHAT IF: a molecular modeling and drug design program, J. Mol. Graph. 8 (1990) 52–56.
[29] R. Luthy, J.U. Bowie, D. Eisenberg, Assessment of protein models with three-dimensional profiles, Nature 356 (1992) 83–85.
[30] W. Trager, J.B. Jensen, Human malaria parasites in continuous culture, Science 193 (1976) 673–675.
[31] M. Vedadi, J. Lew, J. Artz, M. Amani, Y. Zhao, A. Dong, G.A. Wasney, M. Gao, T. Hills, S. Brokx, W. Qiu, S. Sharma, A. Diassiti, Z. Alam, M. Melone, A. Mulichak, A. Wernimont, J. Bray, P. Loppnau, O. Plotnikova, K. Newberry, E. Sundararajan, S. Houston, J. Walker, W. Tempel, A. Bochkarev, I. Kozieradzki, A. Edwards, C. Arrowsmith, D. Roos, K. Kain, R. Hui, Genome-scale protein expression and structural biology of *Plasmodium falciparum* and related Apicomplexan organisms, Mol. Biochem. Parasitol. 151 (2007) 100–110.
[32] J.B. Palenchar, R.F. Colman, Characterization of a mutant *Bacillus subtilis* adenylosuccinate lyase equivalent to a mutant enzyme found in human adenylosuccinate lyase deficiency: asparagine 276 plays an important structural role, Biochemistry 42 (2003) 1831–1841.
[33] L.D.Z. Ariyananda, R.F. Colman, Evaluation of types of interactions in subunit association in *Bacillus subtilis* adenylosuccinate lyase, Biochemistry 47 (2008) 2923–2934.
[34] J. Kyte, Mechanism in Protein Chemistry, Garland Publishing, New York, 1995.
[35] F.H. Westheimer, The magnitude of the primary kinetic isotope effect for compounds of hydrogen and deuterium, Chem. Rev. 61 (1961) 265–273.
[36] C.E. Carter, L.H. Cohen, The preparation and properties of adenylosuccinase and adenylosuccinic acid, J. Biol.Chem. 222 (1956) 17–30.
[37] S. Sivendran, R.F. Colman, Effect of a new non-cleavable substrate analog on wild-type and serine mutants in the signature sequence of adenylosuccinate lyase of *Bacillus subtilis* and *Homo sapiens*, Protein Sci. 17 (2008) 1162–1174.
[38] N.A. Larsen, A. Heine, L. Crane, B.F. Cravatt, R.A. Lerner, I.A. Wilson, Structural basis for a disfavored elimination reaction in catalytic antibody 1D4, J. Mol. Biol. 314 (2001) 93–102.
[39] J. March, Advanced Organic Chemistry, John Wiley & Sons, New York, 1992.
[40] J.A. Gerlt, P.G. Gassman, Understanding enzyme-catalyzed proton abstraction from carbon acids: details of stepwise mechanisms for β-elimination reactions, J. Am. Chem. Soc. 114 (1992) 5928–5934.
[41] D.J. Porter, N.G. Rudie, H.J. Bright, Nitro analogs of substrates for adenylosuccinate synthetase and adenylosuccinate lyase, Arch. Biochem. Biophys. 225 (1983) 157–163.
[42] I.I. Nuiry, J.D. Hermes, P.M. Weiss, C.Y. Chen, P.F. Cook, Kinetic mechanism and location of rate-determining steps for aspartase from *Hafnia alvei*, Biochemistry 235 (1984) 168–175.
[43] C.Y. Wu, H.J. Lee, S.H. Wu, S.T. Chen, S.H. Chiou, G.G. Chang, Chemical mechanism of the endogenous argininosuccinate lyase activity of duck lens delta2-crystallin, Biochem. J. 333 (1998) 327–334.
[44] J.P. Richard, T.L. Amyes, Proton transfer at carbon, Curr. Opin. Chem. Biol. 5 (2001) 626–633.
[45] J.P. Guthrie, R. Kluger, Electrostatic stabilization can explain the unexpected acidity of carbon acids in enzyme-catalyzed reactions, J. Am. Chem. Soc. 115 (1993) 11569–11572.
[46] J.L. Brosius, R.F. Colman, A key role in catalysis for His^{89} of adenylosuccinate lyase of *Bacillus subtilis*, Biochemistry 39 (2000) 13336–13343.
[47] J. Jaeken, G. Van den Berghe, An infantile autistic syndrome characterised by the presence of succinylpurines in body fluids, Lancet 2 (1984) 1058–1061.
[48] E.K. Spiegel, R.F. Colman, D. Patterson, Adenylosuccinate lyase deficiency, Mol. Genet. Metab. 89 (2006) 19–31.
[49] T.P. Zimmerman, R.D. Deeprose, Metabolism of 5-amino-1-beta-D-ribofuranosylimidazole-4-carboxamide and related five-membered heterocycles to 5′-triphosphates in human blood and L5178Y cells, Biochem. Pharmacol. 27 (1978) 709–716.
[50] M.F. Vincent, P.J. Marangos, H.E. Gruber, G. Van den Berghe, Inhibition by AICA riboside of gluconeogenesis in isolated rat hepatocytes, Diabetes 40 (1991) 1259–1266.
[51] J.M. Corton, J.G. Gillespie, S.A. Hawley, D.G. Hardie, 5-aminoimidazole-4-carboxamide ribonucleoside a specific method for activating AMP-activated protein kinase in intact cells? Eur. J. Biol. 229 (1995) 558–565.
[52] R. Rattan, S. Giri, A.K. Singh, I. Singh, 5-aminoimidazole-4-carboxamide-1-beta-D-ribofuranoside inhibits cancer cell proliferation in vitro and in vivo via AMP-activated protein kinase, J. Biol. Chem. 280 (2005) 39582–39593.
[53] A. Bahl, B. Brunk, J. Crabtree, M.J. Fraunholz, B. Gajria, G.R. Grant, H. Ginsburg, D. Gupta, J.C. Kissinger, P. Labo, L. Li, M.D. Mailman, A.J. Milgram, D.S. Pearson, D.S. Roos, J. Schug, C.J. Stoeckert Jr., P. Whetzel, PlasmoDB: the Plasmodium genome resource. A database integrating experimental and computational data, Nucleic Acids Res. 31 (2003) 212–215.
[54] B. Srinivasan, H. Balaram, ISN1 nucleotidases and HAD superfamily protein fold: in silico sequence and structure analysis, In Silico Biol. 7 (2007) 187–193.
[55] R. Pesi, M. Turriani, S. Allegrini, C. Scolozzi, M. Camici, P.L. Ipata, M.G. Tozzi, The bifunctional cytosolic 5′-nucleotidase: regulation of the phosphotransferase and nucleotidase activities, Arch. Biochem. Biophys. 312 (1994) 75–80.